ADVANCED SENSOR RESEARCH Open Access
www.advsensorres.com

Fully Printed PTC Based Heat Transfer Sensor Array as Liquid Level Sensor

*Rainer Bäuerle, Pariya Nazari, Johannes Zimmermann, Christian Melzer, Gerardo Hernandez-Sosa, and Wolfgang Kowalsky**

Liquid levels must be monitored in almost any process involving liquids. Most level sensors are mounted inside the vessel containing the liquid. Herein, a fully screen-printed level sensor is demonstrated for external use. It consists of a vertical array of 16 pixels, each comprising a voltage divider of a positive temperature coefficient (PTC) element and a shunt resistor. The self-regulating PTC elements are heated with constant voltage. Heat flow out of the PTCs dictate their resistances and enables inference about their thermal surrounding. Water in a polypropylene container changes voltage levels by (33 ± 2) % compared to air. Applications with a glass container and household oil instead of water are also successfully tested. Both liquids yield a distinctive difference in signal and the sensor determines the height of the oil/water interface as well as the surfaces of the liquid. To further demonstrate the capabilities of the sensor, segregation of a water-oil mixture, slowed by a mixing agent, is observed in real time. This work offers an adaptable and simple alternative for external level sensing.

1. Introduction

Advances in functional printing have led to an emerge of printed electronics. Especially the field of sensorics has benefited from mechanical flexibility and inks with unique features. Additionally, printing allows for fast and low-cost manufacturing.[1,2] As a result, nowadays printed sensors exist for most application, e.g. temperature, light, and level sensing.[3–7] Most of today's liquid level sensors rely on optic or capacitive effects to detect surfaces and interfaces of liquids.[8–17] Fully printed level sensors have been realized.[8,9] While each type of sensors has their own advantages, e.g. high precision or free design choice, there are disadvantages as well, e.g. complex electronics or build-up on the sensor.[14,18] Furthermore, some interface detectors are only tested against clear interfaces between pure single phases. Also, many sensors require direct contact with the medium under test and are intrusive.[3,4,6,9–15] Depending on the liquid, direct contact between medium and sensor can cause quick degradation or destroy the sensor. For some applications, an installation on the outside of an existing setup is desired. Heat can travel through a sufficiently thermally conductive container wall, rendering such sensors capable of non-intrusive setups.[19] This allows heat based sensorics to be used adaptive to existing structures, especially as afterthought solution.

The fully printed liquid level sensor introduced in this work is based on heat flux through the container wall. It combines the temperature sensitivity of a polymeric positive temperature coefficient (PTC) material with the advantages of printed electronics. It is successfully used for interface detection and dispersion segregation observation.

2. Results and Discussion

As the underlying concept, the step-like PTC behavior of a conductive polymer composite (CPC) is used. The main components of CPCs are a conductive filler and an insulating polymer matrix.[20,21] The density of the filler determines the conductivity of the CPC. At low concentrations of the filler, agglomerates and particles of filler material are isolated within the matrix. At the percolation threshold a conductive network starts to form: due to

R. Bäuerle, P. Nazari
Institute of Organic Chemistry
Heidelberg University
Im Neuenheimer Feld 270, 69120 Heidelberg, Germany

R. Bäuerle, P. Nazari, J. Zimmermann, C. Melzer, G. Hernandez-Sosa, W. Kowalsky
InnovationLab
Speyerer Str. 4, 69115 Heidelberg, Germany
E-mail: wolfgang.kowalsky@ihf.tu-bs.de

R. Bäuerle, W. Kowalsky
Institute of High Frequency Technology
Technical University of Braunschweig
Universitätsplatz 2, 38106 Braunschweig, Germany

P. Nazari, G. Hernandez-Sosa
Light Technology Institute
Karlsruhe Institute of Technology
Engesserstr. 13, 76131 Karlsruhe, Germany

G. Hernandez-Sosa
Institute of Microstructure Technology
Karlsruhe Institute of Technology
Hermann-von-Helmholtz-Platz 1, 76344 Eggenstein-Leopoldshafen, Germany

The ORCID identification number(s) for the author(s) of this article can be found under https://doi.org/10.1002/adsr.202400060

DOI: 10.1002/adsr.202400060

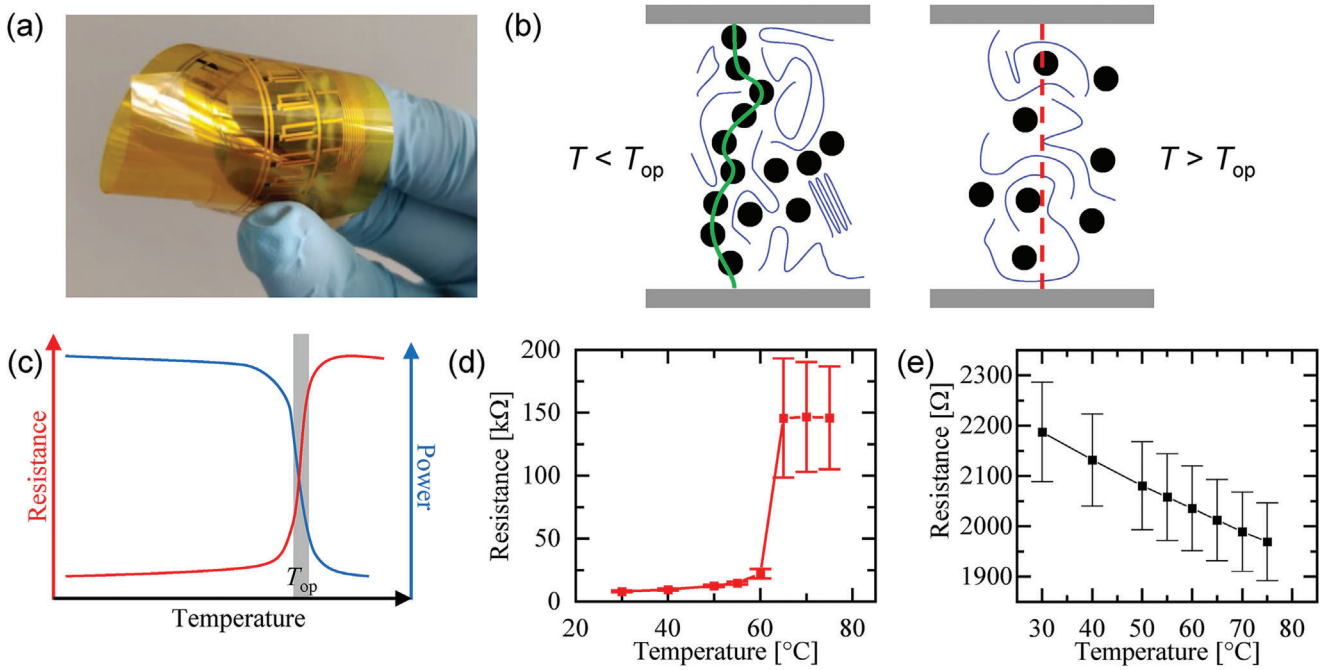

Figure 1. Polymeric PTC effect. a) Photograph of the flexible device developed in this work. b) Schematic of conductive path formed by percolation of conductive particles between contacts below and above operation temperature. c) Typical R-T curve (red) for a polymeric PTC material and the power draw (blue) under constant voltage. Grey rectangle marks the operation temperature. d) Experimental R-T curve for the polymeric PTC material used in this work. e) Experimental R-T curve of shunt resistance SR.

the density of filler particles they are in close proximity or touching, starting to form a connected network. This network allows charge transport from one particle to another throughout the entire material.[21] Thus, conductivity arises from paths of conductive filler particles distributed throughout the CPC. At the percolation threshold, conductivity typically increases several orders of magnitude.[22–24] Additional filler content further increases conductivity albeit its relative change is much less pronounced than at the percolation threshold.[25,26]

The typically observed step-like PTC behavior of some CPC is due to conductive networks with a filler concentration near the percolation threshold. At low temperatures, the conductive network is established, resistivity is low and nearly temperature independent. Heating the composite to the temperature of a phase change, e.g. melting point of the polymer, the arrangement of the polymeric chain changes, leading to the disruption of the conductive network and increasing resistivity.[27] At temperatures above the phase change, the conductive network is destroyed and resistivity accordingly high. Resistivity above phase change temperature is mostly governed by the polymer and thus nearly temperature independent. The scheme explaining this concept is illustrated in **Figure** 1b. As the phase change usually occurs over a small temperature window, resistivity changes step-like as a function of temperature.[28–30] As a result, resistivity is highly temperature dependent in this temperature range.[31,32]

This behavior has been utilized for self-limiting heaters.[33,34] With an applied constant voltage U, the PTC material draws electric power P, according to $P = U^2/R$ with resistance R, and heats up. Upon reaching its operation temperature T_{op} (at which the phase change occurs), resistance R drastically increases and with that, heating power P decreases (Figure 1c). Therefore, power draw of the PTC rapidly drops at T_{op} which prevents the PTC from being heated to temperatures exceeding T_{op}. This way the material is heated only to T_{op} and maintains this temperature.

By choice of material, T_{op} is above ambient temperature T_{am}. Thus, there is heat flow out of the heated PTC. In a steady state, the outgoing heat flow matches the electric heat generation. Consequently, the electric input serves as a measure of heat transfer from the PTC to its surroundings. The outgoing heat flow depends on the thermal properties of the adjacent material. Thus, heat flux out of the PTC material is different for different surrounding materials. This principle is used as a heat flux sensor of which the results are interpreted to differentiate between different surrounding liquids.

Dimensions of the materials play a major role in power consumption, efficiency, and sensitivity. Higher channel width corresponds to added parallel resistors, decreasing resistance, and increasing power consumption, thus introducing more energy into the system under test. Temperature behavior is not dependent on the channel width. Longer channel length corresponds to added serial resistors. This would increase overall resistance. However, as energy is needed to heat the PTC element, which in turn increases its resistance, only a small length of a long PTC element is heated. The remaining length has a constant resistance. To increase the relative resistance change, the channel length should be kept short. For small surface area and suitable printability, channel width and length of the PTC and SR are chosen to 1×1 mm^2 and 5×0.2 mm^2, respectively.

At 30 °C the PTC has a resistance of (8073 ± 658) Ω (Figure 1d). It increases to (149 ± 44) kΩ at 70 °C. The most significant increase in resistance occurs between 62 and 65 °C. The resulting PTC ratio – the ratio of high-temperature resistance to

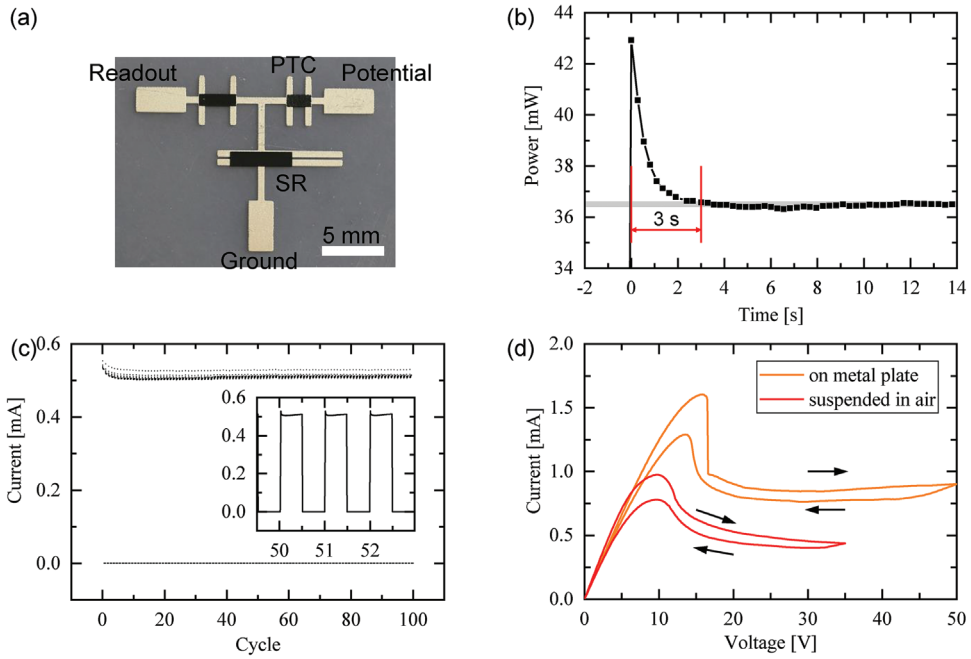

Figure 2. PTC characterization. a) Photograph of a heavily used test pixel containing a PTC resistor and a resistor SR. The additional resistor toward the readout of the test sample was not utilized in the level sensor and is thus ignored. b) Heat-up period of a PTC sample. The sample was suspended in air and supplied with 25 V. After ca. 3 s the sample reaches a constant power draw. c) Current draw during voltage cycling of a PTC sample. The sample was switched between 0 V (0 A) and 30 V (ca. 0.5 A) for 100 times. Lines between data points are removed for better overview. The inset shows a zoom into three cycles. d) I-V curves of a PTC sample. One run was recorded with the PTC element suspended in air and one placed on a metal plate.

low-temperature resistance – is over one order of magnitude (18 ± 6). Figure 1e shows the resistance of a printed shunt resistor SR as a function of temperature. At 30 °C its resistance is at (2188 ± 99) Ω and changes less than 0.15 over the same recorded temperature range, thus it is much less sensitive to temperature changes. Relative to the PTC it can be assumed constant.

Electric characterization of the sensor device was carried out on separate test circuits printed together with the level sensor array (**Figure 2a**). Since SR behaves as an ohmic resistor, the following characterization is carried out over only the PTC part of the device. Figure 2d shows current-voltage (IV) curves of one sample in different thermal surroundings. At low supply voltages (and thus temperature) it behaves ohmic. With increasing voltage, temperature (and thus resistance) increases and current decreases. The voltage at which the behavior changes from constant resistance to power limited depends on the thermal surrounding: in isolating materials (e.g., air) the sensor requires less power to reach and maintain its operating temperature T_{op} and current saturates at lower voltages. Depending on sensor mass and heat flux, it requires some time for the sensor to reach T_{op}. Figure 2b shows the power draw of a sample suspended in air. Power spikes upon applying voltage and decreases over 3 s before reaching a constant level. During this time PTC heats up and its resistance increases until it reaches T_{op}.

The theory of the origin of the PTC effect and quantification thereof is still the topic of ongoing research.[32] Especially reproducibility of the resistance levels after temperature cycling is challenging.[34] In our device with the chosen material, the cycle stability is providing satisfying results. As shown in Figure 2c, switching voltage from 30 to 0 V and back for 100 times has no major effect on the current level.

As demonstrated, the heated PTC can differentiate between different surroundings (Figure 2d, [35]). Applying several such heaters in a vertical array to a container containing a liquid, the readings will vary for different sensor-adjacent liquids or the absence of liquids (**Figure 3a**). For all PTC elements adjacent to the same liquid, the heat flux is the same and thus is the electric energy put into the elements. However, liquids have different thermal properties and accordingly heat fluxes vary. Therefore, an array of PTCs functions as an interface detector or liquid level sensor.

The operation temperature of the PTC is not reached instantly but instead it takes a couple of seconds (Figure 2b). Therefore, any plain switching pixel by pixel would have devastating impact on the response speed of the full array. Consequently, heating and reading of the sensor are separated. This is why a shunt resistor SR is connected in series with each PTC element, forming a voltage divider. The resistor from Figure 1e and Figure 2a is used as SR. With a resistance of SR being small and a constant voltage, the addition of SR has nearly no impact on the power draw of the PTC and heating is undisturbed by the SR. The voltage V_{VD} over the latter is

$$V_{VD} = \frac{R_{SR}}{R_{PTC} + R_{SR}} V_{in} \quad (1)$$

with supply voltage V_{in}, PTC resistance R_{PTC}, and shunt resistance R_{SR}. If R_{SR} is constant and sufficiently small, i.e., $R_{SR} << R_{PTC}$, V_{VD} is inversely proportional to R_{PTC}:

$$V_{VD} \sim 1/R_{PTC} \quad (2)$$

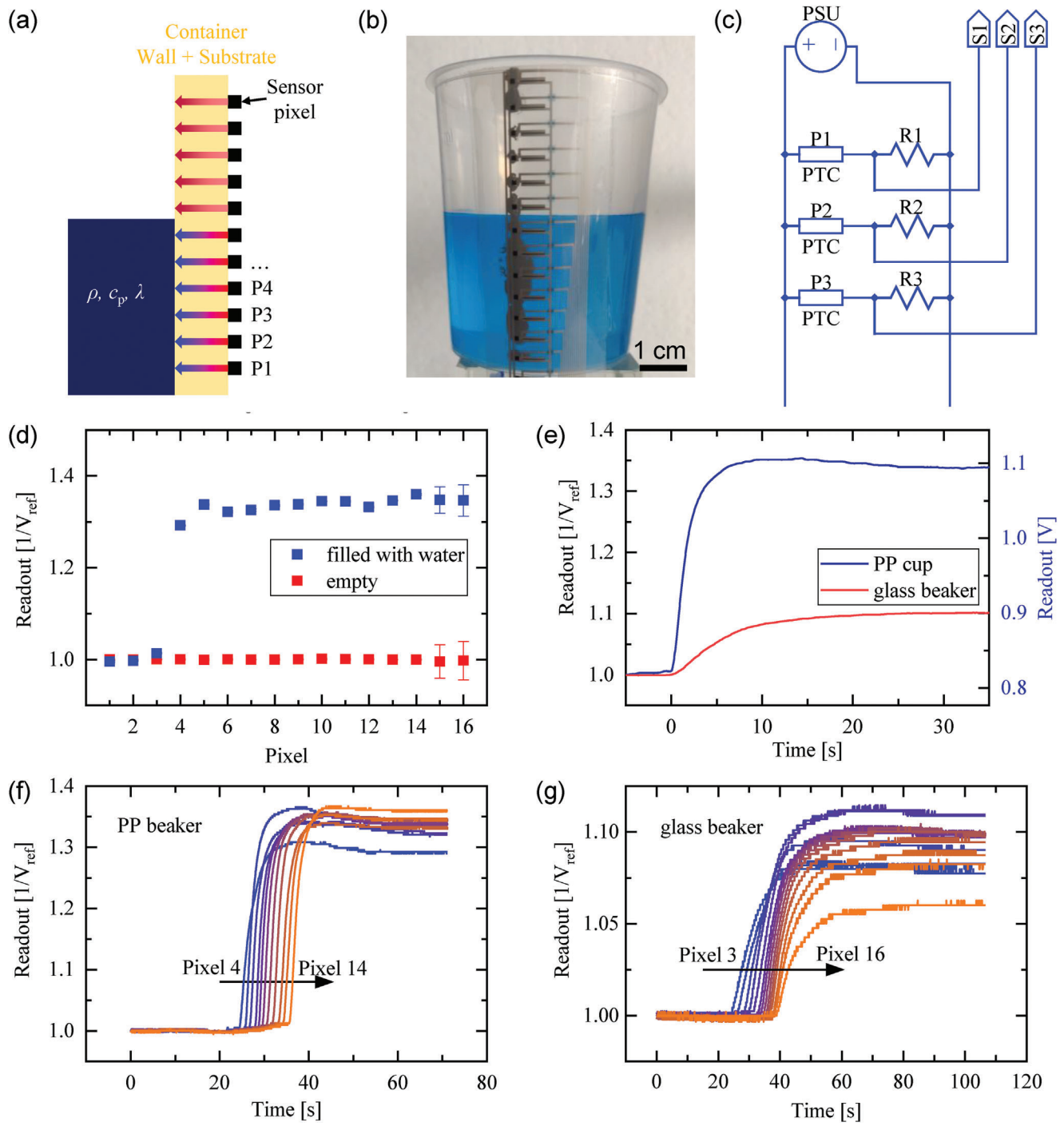

Figure 3. Water level sensing. a) Principle of level sensing. Energy flows from the sensor through the container wall. Depending on the material inside the container the flow rate changes. The symbols ρ, c_p, and λ represent density, specific heat capacity, and thermal conductivity, respectively. b) Sensor applied to a beaker containing (blue colored) water. Grey paste is thermal paste, the black squares are sensor pixels. c) Equivalent circuit of the level sensor. PX and RX form a voltage divider of which the voltage is read as SX. d) Relative signal of pixels 1 to 16 installed on a water filled PP cup. Red dots represent the signal of pixels when the cup is empty (the calibration point) and blue dots show the signal of the water filled cup. Pixels 1–3 are below the bottom of the cup. e) Comparison of PP cup and glass beaker. The exemplary signal is plotted relative to the empty container (left axis). At time t = 0 s the first change in signal occurs. On the right axis the voltage reading for the PP cup is given. Data is Savitzky-Golay smoothed. f) Signal against time of sensor on PP beaker. The water is slowly poured into the beaker over ca. 15 s. g) Signal over time of sensor on glass beaker. The water is slowly poured into the beaker over ca. 15 s. Pixels in f and g are represented by color: from bottom in blue to top in orange.

Table 1. Thermal conductivity and specific heat capacity of relevant materials.

Substance	Thermal conductivity [W m^{-1} K^{-2}]	Specific heat capacity [J g^{-1} K^{-1}]
air	0.026 [36]	1.01 [37]
glass (borosilicate)	1.2 [38]	0.83 [38]
olive oil	0.17 [39]	2.0 [40]
polypropylene	0.22 [41]	2.1 [42]
water	0.6 [39]	4.18 [40]

Any change in thermal surroundings – which results in a change of PTC resistance R_{PTC} – can be quantified by reading the voltage V_{VD} over the shunt resistance R_{SR}. For this reason, signal of the sensor refers to V_{VD} from here on. To obtain multiple sensing points and thus a level sensor, 16 voltage dividers are connected in parallel (Figure 3c).

For detecting the level of a liquid inside a container the sensor is taped on the outside of a 150 ml polypropylene (PP) beaker with a wall thickness of 0.6 mm (Figure 3b). For increased thermal contact a small amount of thermal paste was applied directly onto the PTC elements before taping it to the container. Due to the fabrication there are small variances from pixel to pixel. To compensate for that a calibration of the sensor was done: the recordings of the empty cup are taken, and the data is displayed relative to those readings. The required input voltage depends on the thermal properties of the container and the surrounding and must be chosen on a by-application basis. For a water-air experiment, where the air is the insulator and will yield higher resistance, and thus lower signal, the input voltage V_{in} is slowly increased until a sudden and significant drop in sensor signal is detected. The level sensing experiments in this work are carried out with V_{in} = 30 V.

After taking a calibration reading the cup is slowly filled with water. The signals of the pixels rise after the water reaches the corresponding height. They settle at a relative signal for water of 1.33 ± 0.02 (Figure 3d,f). A clear distinction between relative signals of 1 (air) and 1.33 (water) is visible. As water has both higher thermal conductivity and specific heat capacity than air, see **Table 1**, it is expected to provide increased cooling to the sensor. Therefore, the PTC will be at a lower temperature and lower resistance which in turn results in a higher reading voltage, according to Equation 2. Exemplary readout voltages in Figure 3d are 0.820 V for air and 1.096 V for water. Resolving Equation 1 after R_{PTC}, the resistance of the PTC can be calculated to (78 ± 4) kV and (58 ± 3) kV for air and water, respectively. In this scenario, the sensor successfully and easily finds the water's surface.

The same experiment was carried out with a glass beaker of 3 mm thickness. The relative signal strength of water to air is reduced compared to the PP beaker to 1.09 ± 0.01 (Figure 3e,g). Furthermore, time constant of the sensor (the time it takes to reach 1-1/e of its final value) is almost quadrupled; from (1.7 ± 0.1) s to (6.3 ± 0.4) s in the case of the PP cup and the glass beaker, respectively (**Figure 4b**). With thicknesses of 0.6 mm and 3 mm and a thermal conductivity of 0.22 W m^{-1} K^{-1} and 1.2 W m^{-1} K^{-1} energy flow through the PP and glass container wall should roughly be equal or in favor of glass (367 W m^{-2} K^{-1} versus 400 W m^{-2} K^{-1}). However, due to both higher thickness and thermal conductivity, lateral heat flow inside the container wall is greater in the case of glass. Heat is distributed over a larger area. Thus, point like sensitivity and relative signal strength are reduced. Additionally, with thicker walls and similar volumetric heat capacities (Table 1) heat inertia is higher for the glass container, reducing response speed. However, even with a reduction of both sensitivity and response speed the capability of the sensor to also work with the glass beakers is verified.

The sensor is tested to differentiate between different liquids and detect their respective level. As the difference in thermal properties of the materials is smaller than in the single liquid experiment, so is the expected signal difference. To compensate for that, a different calibration of the sensor was done: two reference points are recorded, i.e., when all pixels are in the same state and surroundings. Unless otherwise noted, the reference points are the empty cup ("0" on the readout scale) and the cup filled with tap water at room temperature ("1" on the scale).

Upon filling the cup with a water/oil mixture the signals for all pixels jump to (1.0 ± 0.1). However, over the next two minutes, the signal of the upper pixels decreases, finally settling at (0.78 ± 0.03) whereas the lower pixels settle after just one minute at (1.02 ± 0.03) (Figure 4a). The one pixel in between steadies at a signal of 0.90. The difference in signal is ascribed to the two different liquids. As water has a higher specific heat capacity as well as higher thermal conductivity than (olive) oil (Table 1) it can absorb more energy faster. This provides increased cooling capacities to our sensor. Thus, it requires more power to keep its operation temperature and the electrical resistance of the PTC part is lower. This leads to a higher signal for water, see Equation 2. The placement of the sensor pixels is in agreement with these results; the pixels with a signal of around 1 are at the height of water – matching the predefined calibration point of "1" –, the pixels with a signal of around 0.8 are at the height of oil, and one pixel sits at the interface and yields the intermediate signal of 0.9. Therefore, the sensor successfully located both interfaces water/oil and oil/air.

To further challenge the sensor, it was tested to track the segregation of an oil-water mixture. Due to a difference in polarity, the liquids usually segregate and develop pure phases. However, it may be of interest to observe the segregation in real time, e.g. in oil production.[43] To slow the segregation of the mixture, a mixing agent was introduced, namely dishwashing detergent. Thanks to its amphiphilic ingredients, the components can form a temporary dispersion.[44] With time however water and oil separate again. Chen et al. carried out thorough tests of this process.[7] To observe the segregation a pre-mixed oil-water mixture is poured into the PP cup (Figure 4e). For increased sensitivity, the pre-mixed liquids are taken as calibration point "1" instead of water. Recordings of all pixels can be found in Figure 4b,d. Immediately after filling, the signal falls for all pixels. Then, pixel by pixel some signals start rising again, the first one 45 seconds after filling. This rise occurs for the pixels from the bottom of the PP cup upwards (Figure 4b,d). After some time, generation of a purer water phase at the bottom of the cup can be seen. This water phase gets more transparent – thus purer – with time. An interface forms between water dominant layer and oil dominant layer. As more and more water falls out of the dispersion the emulsion layer decreases in size and is moved upwards. The movement of the visible interface is also seen in the pixel signal: it changes

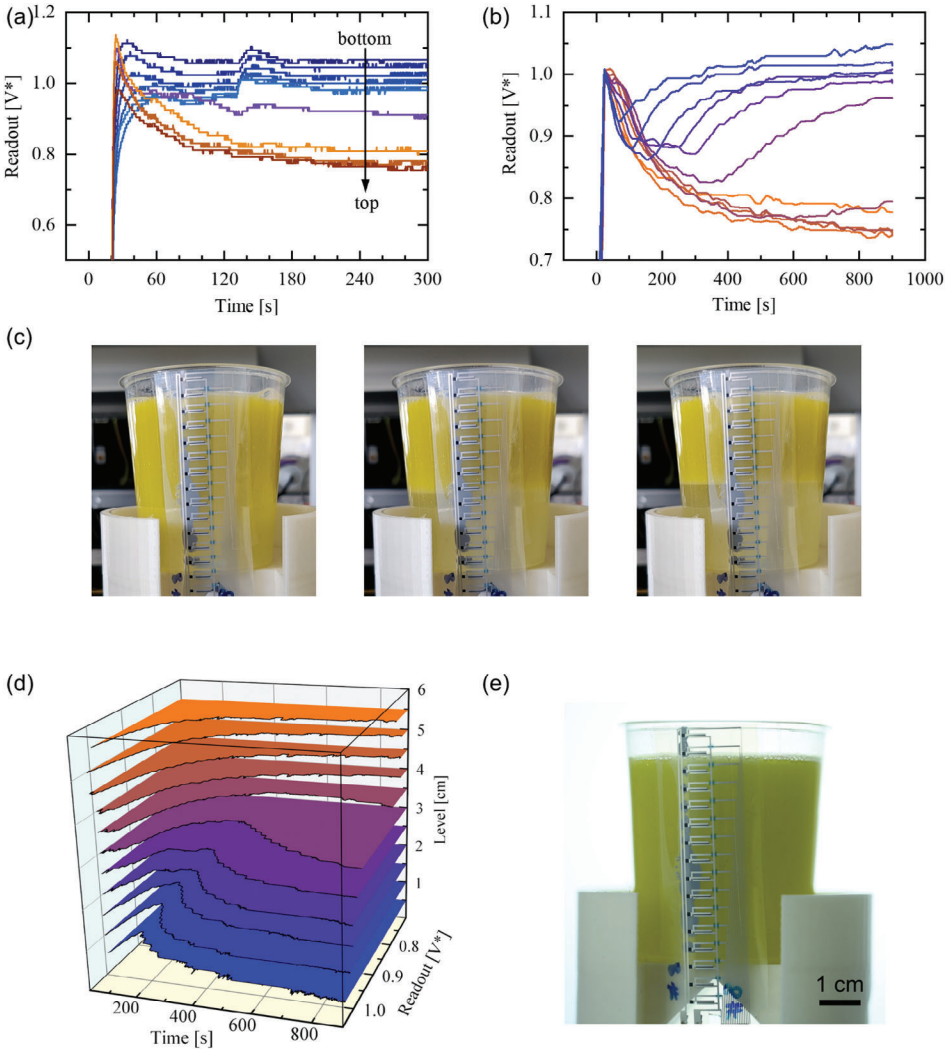

Figure 4. Real-time observation of oil-water-segregation. a) Signal of water/oil mixture without mixing agent. Pixels are colored from bottom to top: at water height in shades of blue from dark to light, at the interface purple, and oil height in shades of orange from light to dark. b) Signal of water/oil mixture with mixing agent during segregation. Pixels are colored from blue at the bottom to orange at the top. c) Lab photographs of the segregation experiment. The photos correspond to 2 min (120 s), 5 min (300 s), and 10 min (600 s) of the experiment in part b. d) Readout of the sensor in 3D representation. The data from b is height-separated to better illustrate the signals of different pixels. Data in b and c is smoothed using a moving average of 50 readings (about 1 s). e) Photo of the test cup in a photo booth immediately after pouring the test mixture in. V* in a, b, and c refers to the two-point calibration.

trend while next to the interface. Pixel 9 is passed by the slow-moving interface over 2 min, at time $t = 400$ s the interface is height-wise roughly in the middle of the pixel. The formerly decreasing signal increases afterwards, see Figure 4b/d. Due to higher water content (and its ability to better conduct and absorb heat) the resistance of the PTC decreases and thus the signal voltage increases. After 900 s, the mostly water neighboring pixels settle at 0.99 ± 0.02 and the oil neighboring pixels settle at 0.76 ± 0.02. Therefore, the sensor distinguishes between the two liquids and yields real-time observation of the segregation.

3. Conclusion

In conclusion, a sensor for precise liquid level and interface detection was successfully demonstrated. It is based on heat flow from an actively heated PTC element into the liquid. A change in the surface level of water at room temperature inside a container can be observed in real-time. Differentiation between water and olive oil is possible not only in the stationary case but also during emulsion segregation. The sensor works from the outside through the container wall. Thus, toxic and chemically aggressive liquids are within the application range of the sensor. The only requirements are good thermal conductivity through the container wall and the liquid(s) being at or below room temperature. However, the latter requirement can be circumvented by use of PTC inks with higher operation temperature. With an operation temperature of 65 °C for the ink used the sensor is also safe to use. Because of the small area and heat capacity it is even safe to the touch, especially through the substrate. Therefore, the sensor provides a low-cost, simple, and safe alternative to

monitor liquid levels and interfaces, observe mixtures, and determine the local gradients of liquid components.

4. Experimental Section

Materials: LOCTITE ECI 8001 E&C, LOCTITE ECI 1010 E&C, LOCTITE ECI 7004HR E&C, and LOCTITE EDAG 451SS E&C were purchased from Henkel AG & Co. KGaA. dielectric. Before applying the inks to the screens, they were thoroughly stirred for several minutes. The PEN substrates were cut to size and heated for 1 h at 120 °C before printing. Testing liquids were tap water from the sink without further treatment, albeit used only after some time to ensure room temperature, typical household olive oil, and standard commercial dishwashing detergent. Thermal paste RS-GCS-040-GNS silicone-free grease from RS Components was used as received.

Device Preparation: The sensors were prepared by screen printing with a Thieme 3010S. The printer is located inside a clean room. First, the contact lines were printed. The silver ink LOCTITE ECI 1010 E&C was dried for 2 min at 80 °C on a hot plate immediately after printing before being annealed for 10 min at 80 °C in an oven. On top, the dielectric layer was printed. It was annealed via UV. To ensure a fully closed dielectric layer two consecutive layers of the dielectric were applied. Then, contacts over the bridges were established by another printed layer with silver ink, annealed as before. Next, PTC ink LOCTITE ECI 8001 E&C was applied. Similar to the silver ink it was dried for 3 min at 90 °C immediately after printing and later annealed for 10 min at 90 °C. Finally, LOCTITE ECI 7004HR E&C as the shunt resistor was printed. This layer was dried and annealed as were the silver layers. Printing parameters were the same for all layers. Squeegee pressure and angle were at 2.3 bar and 73°, respectively. Flood speed was at 300 mm $s^{-}1$ and stroke was at 400 mm $s^{-}1$.

Electric Characterization: I-V and R-T recordings were taken with an Agilent 4155C Semiconductor Parameter Analyzer in conjunction with an Intertek 1000 temperature controller and hot plate. In case of the temperature curves, a delay of minimum 5 min between reaching the target temperature and taking the measurement ensured accurate and homogenous temperature within the sample.

Readout: An Arduino Mega 2560 R3 compatible board with self-written code serves for readout electronics. The reading lines of the sensor are fed to the analog inputs of the Arduino and are read one by one and forwarded over USB to another self-written script on the computer. The reference voltage for analog readings is set by the internal analogReference() to 1.1 V, 2.56 V, or 5 V. Wherever possible, the lowest voltage is used. If the signal exceeds the reference voltage, the next higher is chosen and the experiment repeated. The choice of Arduino Mega also dictates the number of pixels used at the same time, namely 16. Reading speed exceeds 50 Hz.

Level Sensing: For level sensing the sensor was attached to the outside of the container. One stripe of tape on each vertical edge holds the sample in place. The active side of the device, i.e., the side where the printed material is on, is facing the container wall. For increased thermal contact small amounts of thermal paste were put directly onto the PTC before pressing and taping it to the container wall. The containers used in this work are a 150 mL polypropylene beaker with a wall thickness of 0.6 mm and a 250 mL glass beaker (borosilicate 3.3) with a thickness of 3 mm. The liquids were either tested with a thermocouple or kept in ambient conditions for several hours to ensure room temperature.

Sensor Layout: The PTC material LOCTITE ECI 8001 E&C has an active area of $A = 1{\times}1\ mm^2$. The shunt resistor consists of carbon ink LOCTITE ECI 7004HR E&C and has an area of $A = 5{\times}0.2\ mm^2$. For ease of operation, the shunt resistor is connected to ground so the readings can also be taken against ground to get V_{VD}, see Figure 3b. Isolating bridges are centered on the crossing and of $1.5{\times}1.5\ mm^2$. Straight lines connected to the readout have a linewidth of 200 µm while all other contact lines are 500 µm wide. Contact pads for electric power are $7{\times}2\ mm^2$ in size. The overlaps between 1st layer silver lines and contact lines over the dielectric bridges have a length of 500 µm. The pixels have a spacing of 5 mm.

Acknowledgements

The authors thank the German Federal Ministry of Education and Research (BMBF) for the financial support of the 2HORISONS project (03INT606). The authors thank Benjamin Obermayer for his support with the screen-printer.

Conflict of Interest

The authors declare no conflict of interest.

Data Availability Statement

The data that support the findings of this study are available from the corresponding author upon reasonable request.

Keywords

fully printed sensors, interface sensors, liquid level sensors, mixture segregation observations

Received: May 3, 2024
Published online: June 3, 2024

[1] Y. Lu, K. Xu, L. Zhang, M. Deguchi, H. Shishido, T. Arie, R. Pan, A. Hayashi, L. Shen, S. Akita, K. Takei, *ACS Nano* **2020**, *14*, 10966.
[2] L. Yin, J. Lv, J. Wang, *Adv. Mater. Technol.* **2020**, *5*, 2000694.
[3] M. Meribout, A. Al, K. Al, in *Expert Syst. Human, Mater. Autom.* InTech, , **2011**.
[4] R. Casanella, Ó. Casas, R. Pallàs-Areny, in *2006 IEEE Instrum. Meas. Technol. Conf. Proc.*, IEEE, Piscataway, NJ **2006**, pp. 710–713.
[5] S. Mataumoto, W. W. Kang, *J. Dispers. Sci. Technol.* **1989**, *10*, 455.
[6] W. Q. Yang, M. R. Brant, M. S. Beck, *Meas. Sci. Technol.* **1994**, *5*, 1177.
[7] G. Chen, D. Tao, *Fuel Process. Technol.* **2005**, *86*, 499.
[8] M. Kisic, N. Blaz, C. Zlebic, L. Zivanov, M. Damnjanovic, Proc. Int. Spring Semin. Electron. Technol, **2015**, 472.
[9] D. Paczesny, G. Tarapata, M. Michał, R. Jachowicz, *Procedia Eng* **2015**, *120*, 731.
[10] B. Yun, N. Chen, Y. Cui, *IEEE Photonics Technol. Lett.* **2007**, *19*, 1747.
[11] Q. Liu, T. Liu, T. He, H. Li, Z. Yan, L. Zhang, Q. Sun, *Opt. Express* **2021**, *29*, 11538.
[12] S. Mann, S. Lindner, F. Barbon, S. Linz, A. Talai, R. Weigel, A. Koelpin, in *2014 IEEE Top. Conf. Wirel. Sensors Sens. Networks*, IEEE, Piscataway, NJ **2014**, pp. 4–6.
[13] M. Takeda, Y. Matsuno, I. Kodama, H. Kumakura, C. Kazama, *IEEE Trans. Appl. Supercond.* **2009**, *19*, 764.
[14] J. Hong, Y. S. Chang, D. Kim, *Meas. Sci. Technol.* **2010**, *21*, 105408.
[15] B. D. Zimmermann, T.-S. Yang, T. C. Anderson, Liquid Level Sensor Using Thick Film Substrate, US 7596998 B2 **2009**.
[16] S. Srisai, S. Harnsoongnoen, *Int. J. RF Microw. Comput. Eng.* **2021**, *31*, e22557.
[17] D. Mukherjee, N. Sen, K. K. Singh, S. Saha, K. T. Shenoy, P. P. Marathe, *Chem. Eng. Sci.* **2021**, *236*, 116510.
[18] F. A. Khan, A. Yousaf, L. M. Reindl, in 2016 Eur. Freq. Time Forum, IEEE, **2016**, pp. 1–4.
[19] G. Dour, M. Dargusch, C. Davidson, A. Nef, *J. Mater. Process. Technol.* **2005**, *169*, 223.
[20] Y. Huang, S. Kormakov, X. He, X. Gao, X. Zheng, Y. Liu, J. Sun, D. Wu, *Polymers (Basel)* **2019**, *11*, 187.
[21] D. M. Bigg, *Adv. Polym. Technol.* **1984**, *4*, 255.

[22] J.-I. Kim, P. H. Kang, Y. C. Nho, *J. Appl. Polym. Sci.* **2004**, *92*, 394.
[23] S. Park, M. Seo, J. Lee, *Carbon Lett.* **2001**, *2*, 159.
[24] Y. Zeng, G. Lu, H. Wang, J. Du, Z. Ying, C. Liu, *Sci. Rep.* **2014**, *4*, 6684.
[25] Y.-D. Shi, J. Li, Y.-J. Tan, Y.-F. Chen, M. Wang, *Compos. Sci. Technol.* **2019**, *170*, 70.
[26] P. Nazari, R. Bäuerle, J. Zimmermann, C. Melzer, C. Schwab, A. Smith, W. Kowalsky, J. Aghassi-Hagmann, G. Hernandez-Sosa, U. Lemmer, *Adv. Mater.* **2023**, *35*, 2212189.
[27] H. Deng, T. Skipa, R. Zhang, D. Lellinger, E. Bilotti, I. Alig, T. Peijs, *Polymer (Guildf)* **2009**, *50*, 3747.
[28] Z. Chen, P.-C. Hsu, J. Lopez, Y. Li, J. W. F. To, N. Liu, C. Wang, S. C. Andrews, J. Liu, Y. Cui, Z. Bao, *Nat. Energy* **2016**, *1*, 15009.
[29] J. Jeon, H.-B.-R. Lee, Z. Bao, *Adv. Mater.* **2013**, *25*, 850.
[30] K. Chu, S.-C. Lee, S. Lee, D. Kim, C. Moon, S.-H. Park, *Nanoscale* **2015**, *7*, 471.
[31] W. Cheng, S. Yuan, J. Song, *Energy* **2014**, *74*, 447.
[32] Y. Liu, E. Asare, H. Porwal, E. Barbieri, S. Goutianos, J. Evans, M. Newton, J. J. C. Busfield, T. Peijs, H. Zhang, E. Bilotti, *Compos. Part A Appl. Sci. Manuf.* **2020**, *139*, 106074.
[33] I. Ali, A. Shchegolkov, A. Shchegolkov, N. Zemtsova, V. Bogoslovskiy, G. Shigabaeva, E. Galunin, I. Hussain, A. S. A. Almalki, M. A. Alsharif, M. I. Alahmdi, *Polym. Eng. Sci.* **2022**, *62*, 730.
[34] L. Chen, J. Zhang, *J. Appl. Polym. Sci.* **2021**, *138*, 49677.
[35] M. Horn, L. Umar, H. Ruser, in *IMTC/2002. Proc. 19th IEEE Instrum. Meas. Technol. Conf. (IEEE Cat. No.00CH37276)*, IEEE, **2002**, pp. 415–419.
[36] K. Kadoya, N. Matsunaga, A. Nagashima, *J. Phys. Chem. Ref. Data* **1985**, *14*, 947.
[37] J. Hilsenrath, C. W. Beckett, W. S. Benedict, L. Fano, H. J. Hoge, J. F. Masi, R. L. Nuttall, Y. S. Touloukian, H. W. Woolley, *Circular of the Bureau of Standards No.: Tables of Thermal Properties of Gases Comprising Tables of Thermodynamic and Transport Properties of Air, Argon, Carbon Dioxide, Carbon Monoxide Hydrogen, Nitrogen, Oxygen, and Steam*, Commerce Department, National Institute Of Standards And Technology (NIST), Gaithersburg, MD, USA **1955**.
[38] A. G. Schott, BOROFLOAT 33 – Technical Data, SCHOTT Technical Glass Solutions GmbH, Jena, Germany **2019**.
[39] O. K. Bates, *Ind. Eng. Chem.* **1933**, *25*, 431.
[40] C. Peri, *Extra-Virgin Olive Oil Handb*, John Wiley & Sons, Ltd, Chichester, UK **2014**, pp. 349–360.
[41] A. Patti, D. Acierno, Polypropylene – Polymerization and Characterization of Mechanical and Thermal Properties, IntechOpen, London, UK **2020**.
[42] U. Gaur, B. Wunderlich, *J. Phys. Chem. Ref. Data* **1982**, *11*, 313.
[43] H. K. Abdel-Aal, M. A. Aggour, M. A. Fahim, *Petroleum and Gas Field Processing*, CRC Press, Boca Raton, FL, USA **2003**.
[44] K.-Y. Lai, *Liquid Detergents*, CRC Press, Boca Raton, FL, USA **2005**.